International Journal of Scientific Research and Management (IJSRM)
||Volume||10||Issue||12||Pages||CE-2022-28-45||2022||
Website: www.ijsrm.in ISSN (e): 2321-3418
DOI: 10.18535/ijsrm/v10i12.ce01

Numerical study of the filtering barriers influence to contain aerated particulate systems

[1]Andreza Porto Moura, [1]Aureo Alves de S. Neto, [2]Eduardo J. S. Fonseca, [3]Vanderson B. Bernardo, [1,3]José L. S. Duarte, [2]Laís F. A. M. Oliveira, [1]Leonardo M. T. M. Oliveira.

[1]Technology Center of Federal University of Alagoas, Av. Lourival Melo Mota, s/n, Campus A.C. Simões, Tabuleiro do Martins, Maceió-AL, 57072-970, Brazil.
[2]Physics Institute of Federal University of Alagoas, Av. Lourival Melo Mota, s/n, Campus A.C. Simões, Tabuleiro do Martins, Maceió-AL, 57072-970, Brazil.
[3]Chemistry and Biotechnology Institute of Federal University of Alagoas, Av. Lourival Melo Mota, s/n, Campus A.C. Simões, Tabuleiro do Martins, Maceió-AL, 57072-970, Brazil.

Abstract
Since the high rate of viral proliferation caused by Covid-19, it was observed that microdroplets with a pathogenic load can remain floating when in confined environments due to their low densities. They are also subject to being transported very easily when in open environments, becoming potential agents of infection. It has motivated several researchers in the field of particulate systems to try understand how particles behave in more extreme conditions. Bearing in mind that the materials currently used have a low retention yield for liquid droplets, and that protection barriers against pathogens are present both in daily use in hospital application, from diagnosis to treatment, this work simulated computationally, in a Eulerian-Eulerian approach, fluid particle retention efficiency in filter films. The simulated results indicated the high degree of retention of the filtering medium and the dependence of its saturation on the particle diameter and flow velocity, in which the greater the initial flow velocity and larger particles, the faster the saturation and detachment of particles, reducing the filter medium containment capacity. However, the results indicated that even so, retainer materials are efficient in reducing the proliferation of pathogenic loads.

Introduction

Materials for particle filtration have been widely used in several operations of the industry for solid-solid and fluid-solid separation systems. [1,2]. In addition, both in this and in the public health sectors, filter media appear in the form of collective and individual protection equipment in the prevention of respiratory risks due to the different types of contaminating particles to which these professionals are subject [3].

Current events relating to the COVID-19 pandemic have led International Commission on the Futures of Education [4] to classify this period as the greatest public health crisis of the century, which has been causing social, economic and educational disturbances to billions of people in the world due to the high speed of spread of the pathogen and the ability to cause deaths in vulnerable populations.

Insufficient scientific knowledge about the virus has generated uncertainty about what would be the best strategies to be used to face the pandemic in different parts of the world [5], and in this way, several agencies, such as the World Health Organization and the Centers for Disease Control in the United States, have recommended social distancing and the use of face masks as a method to contain the spread [6, 7].

According to Fillingham et al. [8], the use of personal protective equipment (PPE) can help reduce the viral load in contact with people in confined environments, in addition to other collective protection equipment, such as barriers, also having proven efficiency in minimizing dispersed bioaerosols [9]. Besides that, according to Howard et al. [10], in closed environments, it is possible to have suspended particles with a size smaller than or equal to 1 μm, being potential contaminants even with PPE in constant use. Currently, it is known that the efficiency of masks, uniforms and barriers against droplets and bioaerosols in the air is a function of the type of material and their constituent layers, ranging from 50±7 to 97±2% retention for particles up to 300 nm [11].

Tcharkhtchi et al. [12] studied the filtration efficiency and penetration mechanisms of particles in different types of masks and indicated that surgical and cloth masks are not very efficient for particles in the nanometer scale, filtering only micrometers. The respiratory ones, on the other hand, showed a high efficiency of retention of nanometric particles, although they are not popular due to the discomfort of use. The authors also attested that the parameters with the greatest influence on penetration were the particle size and its flow velocity. The mechanisms involved in the transport of pathogens through the filter media were interception, gravity and inertia for particles larger than 0.5 microns, while for particles smaller than 0.2 microns, diffusion was dominant. At high flows interception is the most present penetration parameter and at low flows diffusion and electrostatic interaction.

Other studies have already indicated that the dispersion characteristics, and possible spread of infectious diseases, are highly dependent on the diameter and flow velocity of the droplets [13]. Thus, using computational fluid dynamics (CFD) numerical simulation, the dispersion of particles in the air can be analyzed and predicted.

Fluid dynamic modeling can help identify properties of these materials, such as porosity, particle containment capacity in the porous medium and its permeability. Tang and Guo [14] suggested that one of the best modeling conditions to simulate particle dispersions is based on the Euler-Euler approach considering droplets as dispersed and polydisperse fluids (with clusters of varying diameters), in a particle model, in addition to using the RANS turbulence model k-ε type. Leonard et al. [15] used CFD to simulate the flow of aerosols through a surgical mask on a human face, including its average permeability and porosity characteristics, as well as gaps between the face and the PPE. In their simulations, it was noted that the surgical masks had a filtration capacity of up to 88.8% in particle capture and strong dependence on the particle diameter involved, showing lower efficiencies when these were smaller than 0.8 microns.

Qian et al. [16] developed a numerical simulation of the gas-solid flow inside a fibrous filter medium by CFD-DEM coupling, and evaluated the influence of the structural parameters of the fibers in terms of pressure drop, filtration efficiency, particle deposition and agglomeration. The authors found that with the increase in filtration time, accumulation and piling of particles occurs, increasing the pressure drop, which also increases as a function of the morphology of the fibers, that is, the greater their diameters, the greater the pressure drop.

More recently, and turning to the current pandemic scenario, Mariam et al. [17] simulated in CFD the transmission of pathogenic particles of COVID-19 under different propagation mechanisms, in a confined environment considering the presence of two people at 2.0 meters apart, and assuming internal air movement through different entrances. The authors identified that the receptor was reached by the particles even under the condition of lower ejection speed, and these remained suspended in the environment even after 30 minutes after being launched.

Although the cited works provide enough information to believe that facial PPE is safe and has the potential to mitigate the effects of a pandemic where most contagions occur through the oral and respiratory routes [18], in some regions of the world there is still resistance on the part of the population to credit the functional effect of the use of this equipment. At this point, the study of the filtering behavior of thin and standardized layers of materials subject to the flow of particles under conditions similar to those expelled by the human body, can help the development of advanced filtering media formed of varied materials and with increasing retention potentials.

Thus, the present work aims the numerical simulation of filtering element retention efficiency with characteristics of a single layer of cotton surgical masks in a wind tunnel flow, via CFD Software, analyzing aspects such as the absence and presence of the medium filter, influence of particle size and flow velocity on the filtration process. It is expected, with this, to obtain more elements capable of ratifying the positive influence that PPE's have in controlling the spread of pathogens among people and to contribute to government agencies for their decision-making when faced with pandemic and epidemic scenarios.

Materials and Methods

The manuscript required the proposition of a domain to be treated as a control volume, numerical mesh generation, mathematical modeling to represent the expelled system and the filter medium, and boundary conditions adopted for the simulations.

Problem Geometry

To elaborate the domains that represent the problem, two different cases were considered. The first case, shown in Figure 1(a), presents a small-scale wind tunnel, where there is an inlet region where the fluids are inserted into the system with a predetermined velocity, followed by an area where the fluids can circulate freely inside until the exit face.

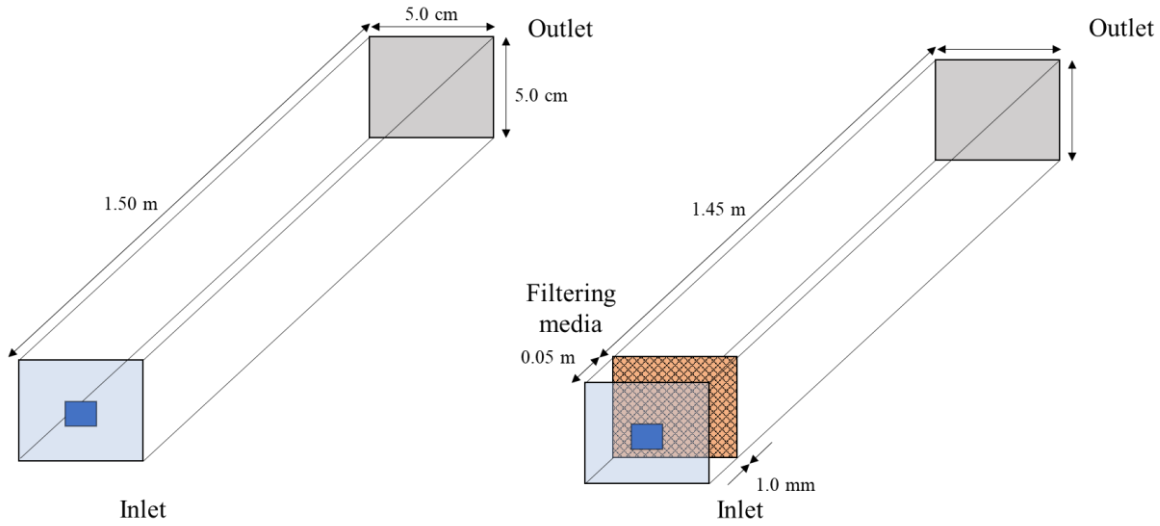

Figure 1: (a) Domain representation without filter media; (b) Representation of the domain with filter media.

The length between the entrance and the exit is 1.5 meter, which is the appropriate value for distancing between people in cases of pandemics such as COVID-19, according to Australian Government Department of Health [19]. The fluid entry area is 1.34 cm², a value similar to the average cross-sectional area of human nostrils according to Gomes et al. [20]. In the other case, according to Figure 1(b), there is the presence of the filter medium in the domain. The input and output regions have the same dimensions mentioned previously.

Computational mesh

Meshes were generated using structured hexahedral elements. Quality tests were performed on these meshes to verify the best choice in morphological terms based on the 'quality' criterion available in the software, which can vary between 0 and 1, in which Ansys ICEM CFD considers good quality values greater than 0.3. The closer to 1, the morphological distribution of elements with excellent quality is obtained. The results achieved for the two meshes developed are shown in Table 1.

Table 1: Quality characteristics of numerical meshes.

Quality parameters	Without filtering media	With filtering media
Nodes number	72,600	203,793
Elements number	79,139	223,227
Quality	1.0	1.0

Mathematical Modeling

Aiming to represent the relevant phenomena to the problem, a modeling based on the conservation equations for flows in porous media was applied and, for such, the following simplifications were adopted:

• Newtonian fluids;
• Compressible flow for the gaseous phase and incompressible for the liquid phase;
• Homogeneous and isotropic porous medium;

• Flow in transient regime;
• Absence of chemical reactions;
• Heterogeneous modeling, with equations solved for each phase;
• Impermeable and static wind tunnel walls;
• Two-phase flow (liquid particles and air) with application of the multiphase particle model;
• The possibility of coalescence between the liquid phase particles was neglected.

The definition of mass conservation in fluid and porous media was applied according to Equations (1) and (2) respectively:

$$\frac{\partial}{\partial t}(\gamma \rho_\alpha r_\alpha) + \nabla.\left(\boldsymbol{K}.\rho_\alpha r_\alpha \vec{U}_\alpha\right) = S_{M\alpha} \quad (1)$$

$$\frac{\partial}{\partial t}(\rho_\alpha r_\alpha) + \nabla.\left(\rho_\alpha r_\alpha \vec{U}_\alpha\right) = 0 \quad (2)$$

In these equations, ρ represents the fluid specific mass, γ is the filtering media porosity, $\vec{U}$ is the velocity vector, and U_x, U_y, e U_z are the components of this vector, and **K** refers to the second order tensor of "porosity area" which is represented as isotropic. The indices of α represent the same properties cited for a given phase α flowing in the fluid medium, and the term r_α indicates the volumetric fraction of this phase, where $\sum_{\alpha=1}^{\alpha=N} r_\alpha = 1$, where N is the total number of phases present. The first term of the equation refers to the accumulation of mass in the pores of the filtering material; the second to the advective term of mass transport across boundaries, governed by the velocity gradient [21].
In the porous medium, a mass source term was also inserted, S_M, in which data from the kinetic equation of absorption of a cotton fabric and water based on Hamdaoui et al. [22] to represent the saturation of the material over time, q (mg/g), with the collision of particles as indicated by Equation (3). Thus, the source term can be represented by Equation (4).

$$q = k_1 q_e e^{-k_1 t} \quad (3)$$

$$S_M = -\left(1 - V_p\right).\rho_{sol}.q \quad (4)$$

Where k_1 is the kinetic adsorption constant (s^{-1}), q_e is the amount of fluid adsorbed by the material at equilibrium (mg/g), t is the time (s), V_p is the pore volume occupied by fluid and ρ_{sol} is the density of filtering material (kg/m^3).
The momentum conservation equations were applied as described in Equations (5) and (6) for porous and fluid media respectively, where the first term represents the accumulation of momentum in the system, the second represents momentum transport, the third indicates the momentum contribution by diffusion, Where μ_e represents the effective viscosity of fluids, S_{Mt} is the momentum source term ∇p is the pressure gradient involved in the process. The term$(\Gamma^+{}_{\alpha\beta}\vec{U}_\beta - \Gamma^+{}_{\beta\alpha}\vec{U}_\alpha)$ in turn, also a diffusion term, represents the mass transfer between the phases, considering the fraction that is transported from α to β, and from β to α.

$$\frac{\partial}{\partial t}\left(r_\alpha \gamma \rho_\alpha \vec{U}_\alpha\right) + \nabla.\left(r_\alpha \rho_\alpha.\left(\boldsymbol{K}.\vec{U}_\alpha\right)\otimes\vec{U}_\alpha\right)$$
$$-\nabla.\left(r_\alpha \mu_e \boldsymbol{K}.\left(\nabla\vec{U} + \left(\nabla\vec{U}\right)^T - {}^2/_3\,\delta\nabla\vec{U}\right)\right) = -\gamma\nabla p_\alpha \quad (5)$$

$$\frac{\partial}{\partial t}\left(r_\alpha \rho_\alpha \vec{U}_\alpha\right) + \nabla.\left(r_\alpha \rho_\alpha.\vec{U}_\alpha\otimes\vec{U}_\alpha\right) - \nabla.\left(\mu_e r_\alpha.\left(\nabla\vec{U}_\alpha + \left(\nabla\vec{U}_\alpha\right)^T\right)\right) = \sum_{\beta=1}^{N}\left(\Gamma^+{}_{\alpha\beta}\vec{U}_\beta - \Gamma^+{}_{\beta\alpha}\vec{U}_\alpha\right) - r_\alpha\nabla p_\alpha \quad (6)$$

The k-ε turbulence model was also applied for the continuous air phase, a widely used two-parameter and two-equation model [23, 24], que resolve para k a energia cinética turbulenta e para ε a taxa de dissipação de energia turbulenta [21]. As for the mixture containing air and particles, as it is a multicomponent fluid, the dispersed phase zero equation model was applied, which is also solved for two parameters, which solves the turbulent kinematic viscosity of the dispersed phase relating it to the Prandlt number turbulent and the turbulent kinematic viscosity of the continuous phase [21].
In the generated multiphase system, the particle model was used, and the drag contribution suffered by the particles was indicated by the Ishii Zuber model, which considers that these are not necessarily spherical, but the drag depends on their surface format, mainly in the representation of flowing particle systems [25], being able to be a good representation for those released in the air in sneezing and coughing within the considerations made.

Boundary and initial conditions

The filtering material was inserted into the software as a solid medium containing a porosity of 9.1%, this value for filtering cotton surgical masks, as described in the work of Jakšić e Nikola [26]. The materials used in the simulated domain contain a dispersed fluid phase with similar characteristics to expiratory particles in phenomena such as coughing and sneezing, Table 2, and a continuous gaseous phase similar to air. From data obtained by Han, Weng e Huang [13] e Kotb, Khalil [28], were used, 3.4 m/s, 10 m/s, 15 m/s e 25 m/s for the injection velocities of the fluid particles in the domain during an interval of 0.5 seconds, observing the flow for a total time of 1.0 seconds. The described speed of a sneeze ranges between 10 and 50 m/s, while 10 m/s is the approximate value of particles expelled by coughing [13, 28]. Thus, the work also evaluated the behavior at an intermediate value, 15 m/s, and, to simulate the behavior of particle transport from speech, it was simulated at 3.2 m/s [29]. The diameter of these varied by 10 µm, 74.4 µm and 100 µm. The value of 74.4 µm represents the average diameter of particles expelled in the sneezing process [13], and thus, this work extended the evaluation range to investigate the behavior of mainly smaller particles.
As observed by Tang et al. [28], a human sneeze can vary from 0.06 to 0.3 seconds. Thus, aiming to simulate only a brief period of flow of the air-particle mixture in an attempt to represent a coughing or sneezing phenomenon, a UDF (User Defined Function) in CEL (CFX Expression Language) was inserted to guarantee the representation of a fluid pulse for a short time of 0.5 s, conditioning the flow to cease after this time. Time was extrapolated to simulate a generic case of sneezing, coughing or short speech. For the output, an opening condition with a relative pressure of 0 atm was applied.
A mixture of fluids (air + particles) was created with a proportion of 10% by mass of particles and 90% of air, in order to represent the input fluid in the wind tunnel. The density and viscosity of the particles considered were also related to fluids expelled by the human respiratory system in the form of thicker saliva [30]. The applied fluids properties over the simulation time are shown in Table 2.

Table 2: Properties and proportions of involved fluids.

Fluid	**Density (kg/m^3)**	**Viscosity (Pa.s)**	**Phase proportions**	**Phase type**
Pseud-air	1.29	$1.81.10^{-5}$	Continuous - 1 (m/m)	Gas
pseud-fluid	1100	1.5	Disperse - 1 (m/m)	liquid
Mixture	-	-	Continuous - pseud-air - 0.9 (m/m) Disperse - pseud-fluid – 0.1 (m/m)	liquid-gas ideal mixture

At time equal to zero, the entire domain, both the fluid and the porous part, was set with a relative pressure of 0 atm, and 100% saturation for air, which was considered with zero velocity. A fixed proportion of pseudo-air and mixture of 0.5 for each phase was also maintained in the input condition.

Case studies

Three specific cases were analyzed: in the first, the objective was to understand the influence of the presence of a porous filter medium with a thickness of 1.0 mm in a flow that represented a sneeze at 25 m/s. Thus, for

this analysis, the parameters of velocity similar to that of particles expelled during a sneeze and average particle diameter at 74.4 µm were set, and the application or not of the filter medium was varied.
The second case studied the influence of the flow velocity with the presence of the filter medium, which varied in 3.4, 10, 15 and 25 m/s under constant particle size of 74.4 µm. And finally, the influence of the particle diameter, 1.0, 10 and 74.4 µm, was evaluated in the filtering process under two extreme speeds, 3.4 m/s, representing the droplets flow by speech, and 25 m/s by observing it in a sneeze.

Results and Discussion

Filter medium influence

Figure 2 shows the fluid flow in the windpipe for considerations in a system which there is no filter (Figure 2 - Left) and in the presence of a filter medium (Figure 2 - Right). From Figure 3a, it is possible to see that there is no impediment to the particles flow. In this way, all the fluid injected into the domain follows the natural path to exit region, making the distance of 1.5 m highly filled. The domain containing the filter is shown in Figure 2 - Right, where it expresses the fluid injected and subsequently retained in the filter medium, allowing only small amounts of material to pass through the porous barrier.
However, even if some amount of particles crosses the porous structure, it cannot reach even 30% of the tube length due to the imposed deceleration and retention action, keeping the mixture with the particles concentrated upstream from the filter and up to 35 cm downstream, even after 1.0 second flow. In the system without the retaining medium, it is observed, on the other hand, that after 0.5 seconds there is a low concentration of particles in the initial region of the windpipe, while in intermediate zones and close to the outlet they are more concentrated.

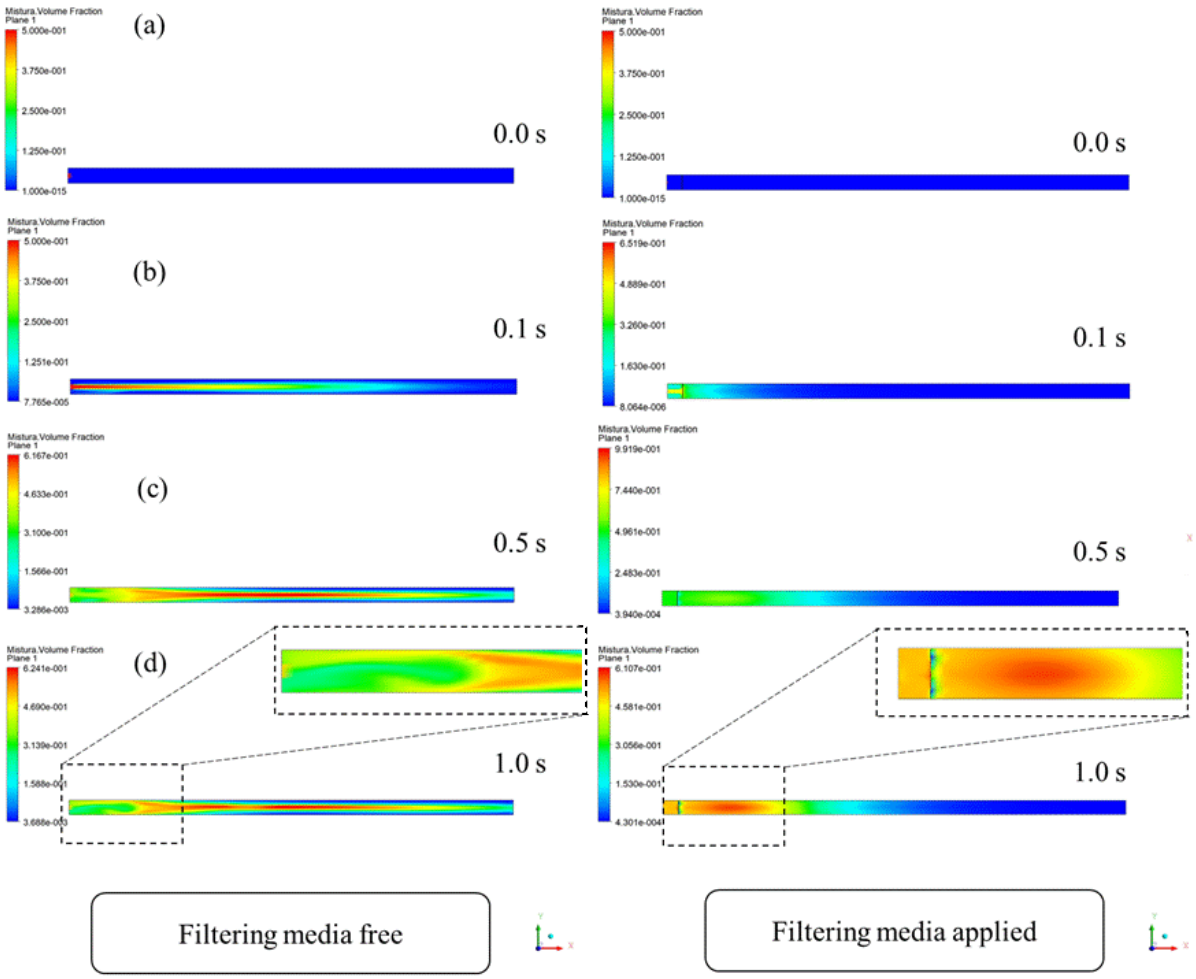

Figure 2: Particle gradient profiles considering the system: Left - without the filter médium; Right - with the filter medium.

In Figure 3, the volumetric percentage of dispersed fluid in the safety region (1.5 meters) with and without the presence of the filter during the simulation time of 1.0 second was plotted. In the system without filter media, a high rate of increase in the amount of particles was observed in the outlet region, reaching a maximum limit of 8.36% at the time of 1.0 s, with some attenuation after that due to the absence of inlet flow and occurred dispersion. In the filtered system, it is evident that there is no significant increase in the rate of rise in the concentration of particles at the outlet, remaining in the range of 0.053% in 1.0 second of flow.

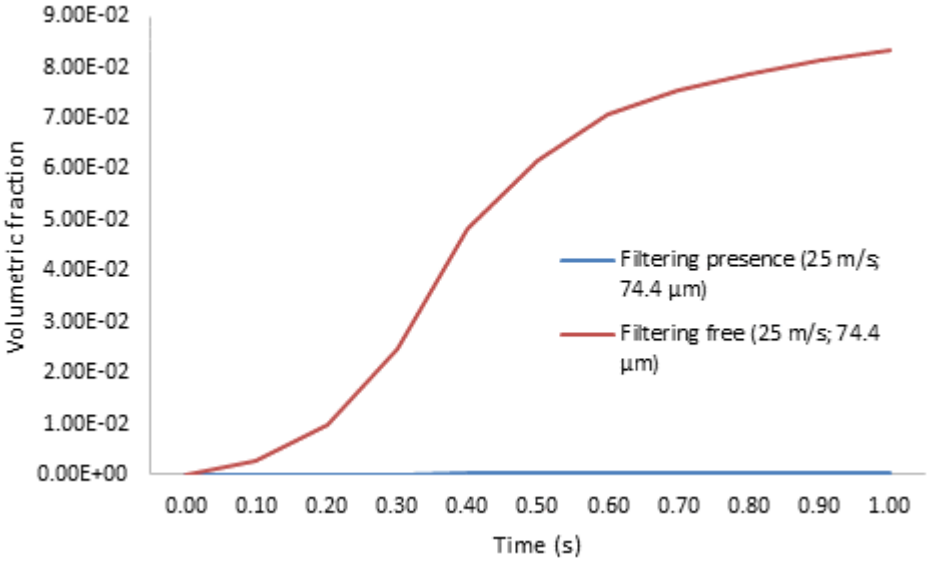

Figure 3: Numerical comparison between the system with and without filter medium as a function of time.

These results are in agreement with experimental tests developed by Sankhyan et al. [31], who evaluated the retention capacity of several cotton matrix masks, in which they obtained 83 to 99% efficiency for N95 respirators.

Velocity influence

For influence of the injection speed of the fluid particles in the domain analysis, the other parameters were fixed. Thus, only the domain containing the filter medium with particles of 74.4 µm in diameter was used. Figure 4 presents the particle saturation gradient advancing in time at the porous and fluid and domain for each tested velocity.

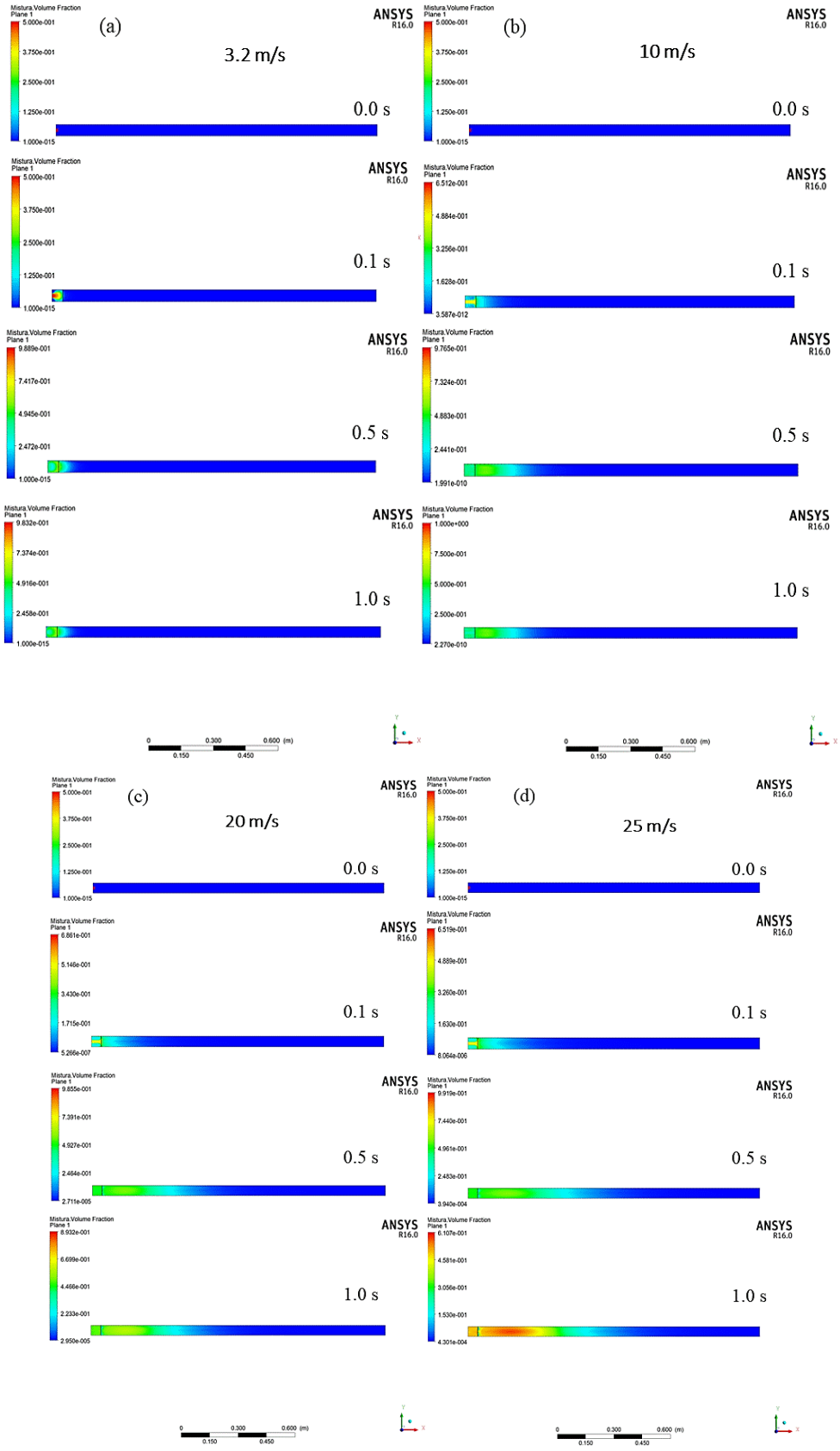

Figure 4: Particle saturation gradients crossing the pore structure and fluid domain at different speeds: (a) 3.2 m/s; (b) 10 m/s; (c) 20 m/s; (d) 25 m/s.

Observing the velocity gradients in Figure 4, it is noted that at speech-related velocities, 3.4 m/s, in 1.0 second there is a great deceleration and accumulation of particles upstream of the filter medium, with a slight passage of particles after this time at only about 5.0 cm in front of the membrane. With the increase in speed to 10 m/s, there is a dispersion of particles downstream of the porous screen of up to 30 centimeters. At 15 m/s this advance reaches 65 cm, and at 25 m/s it reaches 85 cm. It was also evidenced that for the particular case of 25 m/s, representative of a sneeze, although the filter medium generates deceleration and accumulation of particles upstream, it was still possible to notice a high concentration of injector fluid, around 60%, in up to 40 cm downstream of the filter. Figure 5 represents the volumetric fraction of droplets in the event of a sneeze that accumulate in the filter medium over time, depending on the initial flow velocity.

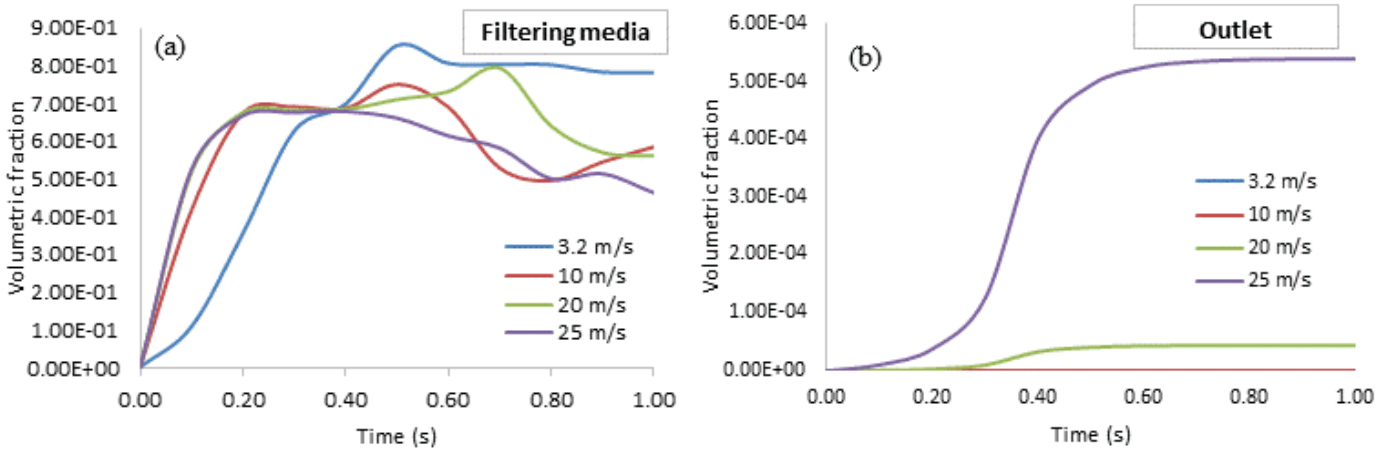

Figure 5: Volumetric fraction of particles in (a) filter media and (b) windpipe outlet as a function of time.

Evaluating the graphs in Figure 5a, one can see how much the injection speed interferes with the volume of fluid accumulated in the filtering material. Up to a time of 0.4 seconds, there is a great increase in the fluid concentration in the filter medium, and after that time, only at 3.4 m/s does the concentration remain around 80% stable, indicating the major retention of the fluids, behavior evidenced in the gradients of Figure 4a. For the other speeds, there was a slight drop in concentration in the filter, suggesting that part of the particles were detached due to the high drag. Figure 5b shows that, although all outflow concentrations were shown to be low, at the velocity of 25 m/s it still reached 0.055% in 1 second, indicating that this fluid spread in environments without circulation could eventually prove to be problematic, especially if the particles are highly transmissible pathogens.

Influence of expelled particles size

Figure 6 allowed the analysis of the volume of fluid expelled under the fixed velocity of 25 m/s considering the variation in the particles diameter. It was observed, as shown in Figure 6a, that for 1 µm particles there was increasing accumulation in the filtering medium, indicating that aerosol particles are likely to sustain and saturate in the presented filter, although the increasing concentration profile indicates that, for times greater than 1.0 second, it is possible that the system saturates and initiates a process of detachment of these particles. Likewise, at a size of 10 µm there is a gradual increase in the volumetric fraction of particles in the filter and, after a maximum of around 0.6 seconds, a slight decay begins. A similar behavior is noted for the 74.7 µm particles, but these reach a maximum volume fraction on the filter at an earlier time of 0.2 seconds, starting then their decay. These results corroborate the idea that larger diameter particles are subject to agglomeration more quickly, occupying the spaces available in the filter medium and, by agglutination, preventing other particles from occupying space in the pores of the material. At the exit of the wind tunnel, as indicated by Figure 6b, it is suggested that only the 74.4 µm particles arrived at higher concentrations of 0.055%, since the others were retained more efficiently in the time of 1.0 s, in addition to are substantially the least dense, suffering dissipation of their little energy in shocks in the porous system.

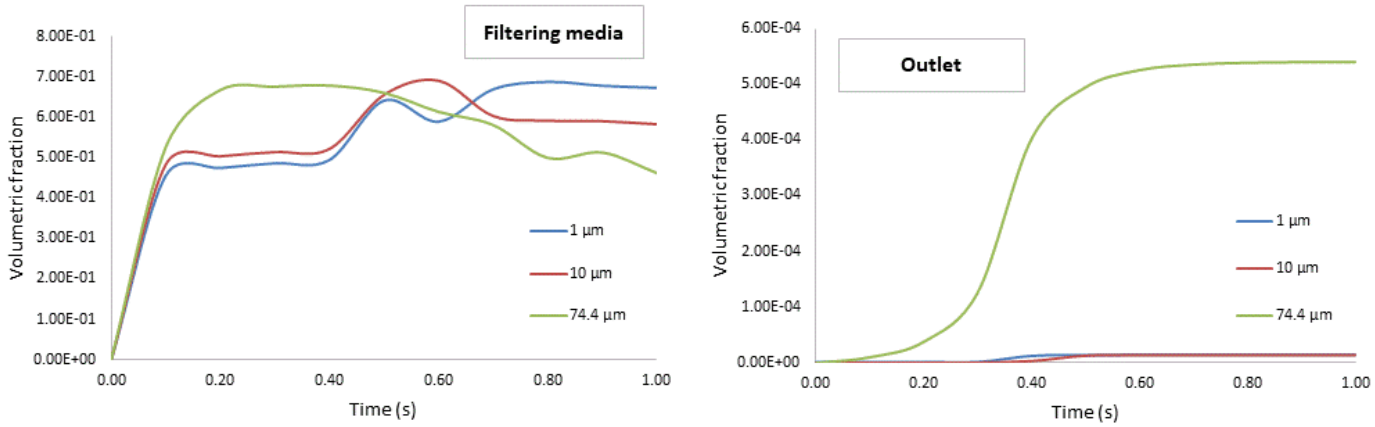

Figure 6: Volumetric fraction in terms of particle diameter in (a) filter media and (b) windpipe outlet for a velocity of 25 m/s.

Figure 7 presents the same comparison of behavior in terms of particle diameter, but regarding to a 3.2 m/s and only for the filter medium. The tube outlet results for all diameters showed a zero amount of particles in the evaluated time of 1.0 second.

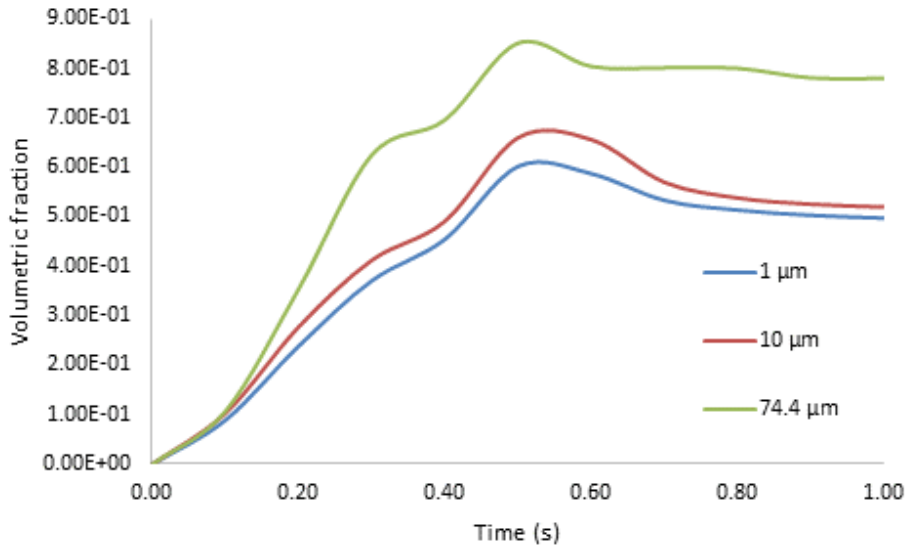

Figure 7: Volumetric fraction in terms of particle diameter in the filter medium for a velocity of 3.2 m/s.

In this case, a proportional relationship between particle diameter and retention was noted. As the particle diameter increases, a greater and faster saturation of the porous medium is observed, supposedly due to the occupation effect, both of the space upstream of the filtering medium, and of the empty spaces contained in the material. With the low flow velocity, it is evident that the profiles assume similar saturation behaviors, with a faster start until close to 0.35 s, a peak at 0.5 s, and finally a stabilized attenuation.

Figures 8 to 11 show the inlet mixture flow plans, with emphasis on the regions immediately upstream and downstream of the filtering body. It can be seen from Figure 8, with the system under a speed of 3.2 m/s and 1 µm, the presence of high vorticity and recirculation of particles upstream from the porous medium, which explains the low rate of adhesion to the pores observed in evaluations previous. It is noted that as the particles recirculate in the entrance region, they lose energy and reduce their speed, to the point where, combined with the flow loss, the circulation becomes extremely slow in 1.0 second, in the range of 0.01 m/s.

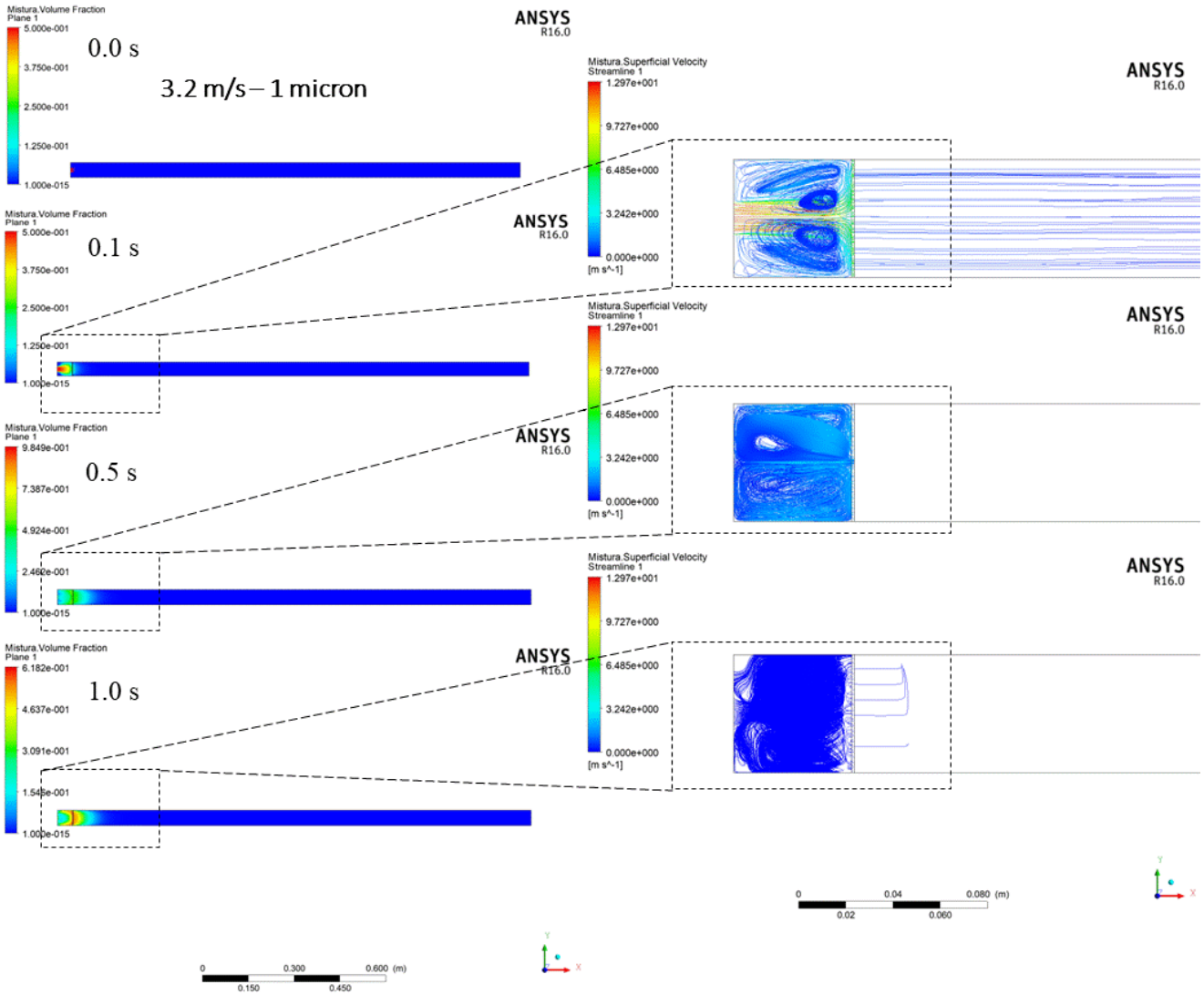

Figure 8: Flow in the windpipe for a velocity of 3.2 m/s at 1 µm particle size.

In Figure 9, the inlet fluid is subject to the same process of generating vortices, recirculation and deceleration, however, it is noted that the particles subject to agglomeration begin the process of detachment and passage through the porous medium, which contributes to reducing the intensity turbulence upstream of the filter medium.

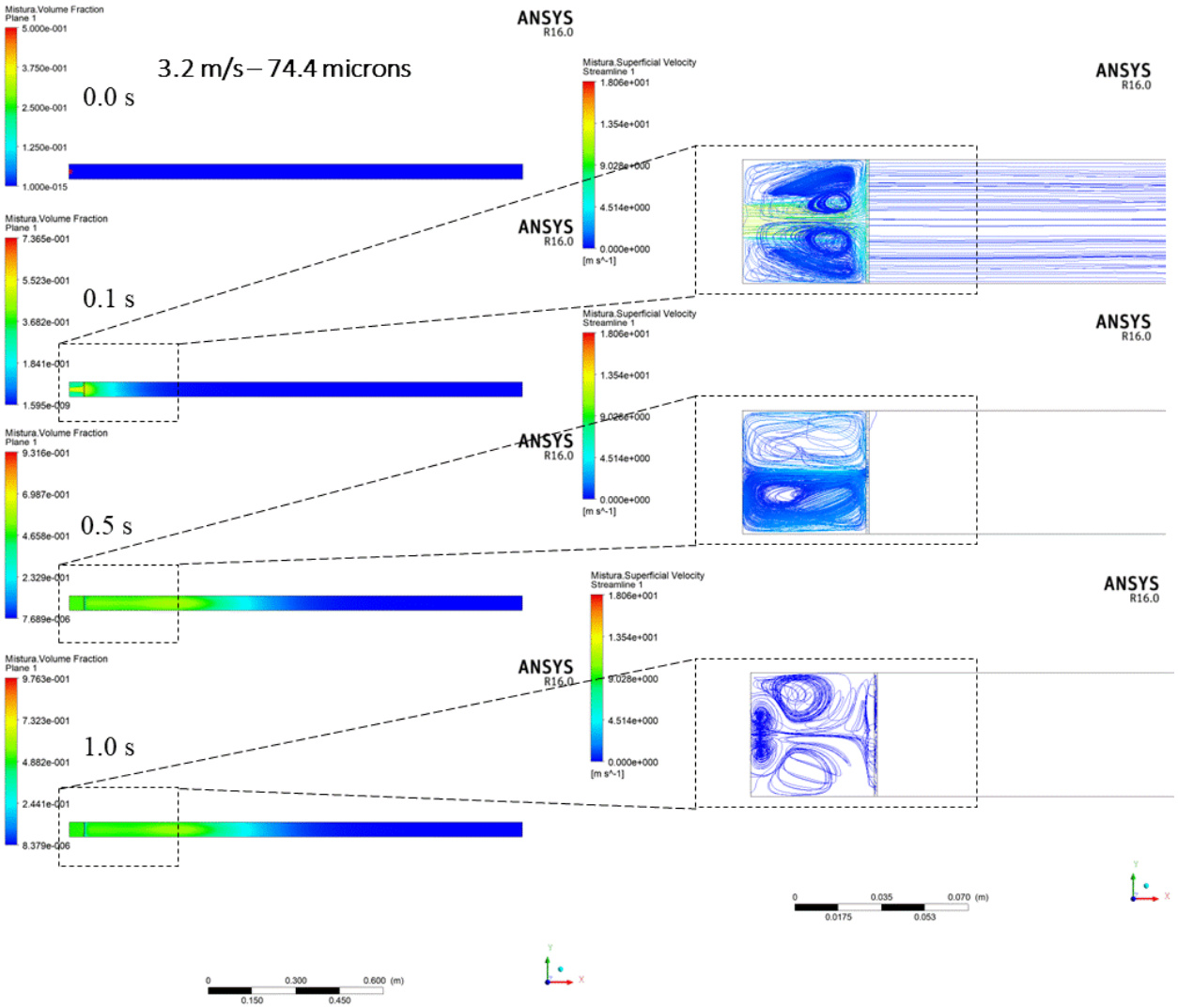

Figure 9: Flow in the windpipe for a velocity of 3.2 m/s at 74.4 µm particle size.

Figure 10 shows that under 25 m/s, 1 µm aerosol particles also generated a turbulence effect upstream, however, due to the high velocity, they tended to accumulate and quickly saturate the central region of the porous medium and initiate the early detachment process. In Figure 11, with particles of 74.4 µm at 25 m/s, it can be seen that two phenomena, agglomeration with detachment and dragging, are present and responsible for ensuring that both the upstream region has recirculation zones smaller than in the other cases analyzed, when the downstream region presents a greater inlet fluid saturation, mainly during the injection process.

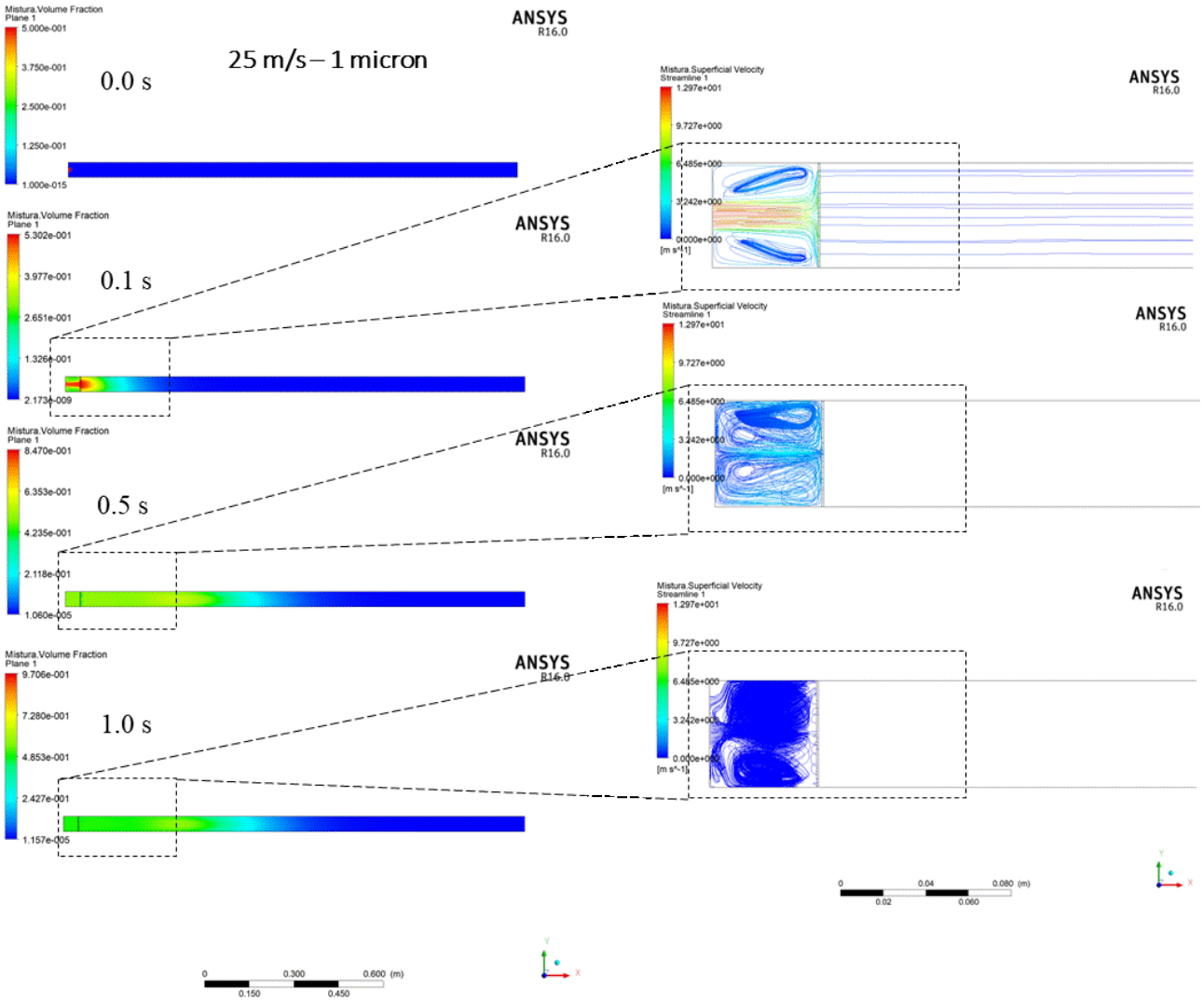

Figure 10: Flow in the windpipe for a velocity of 25 m/s at 1 µm particle size.

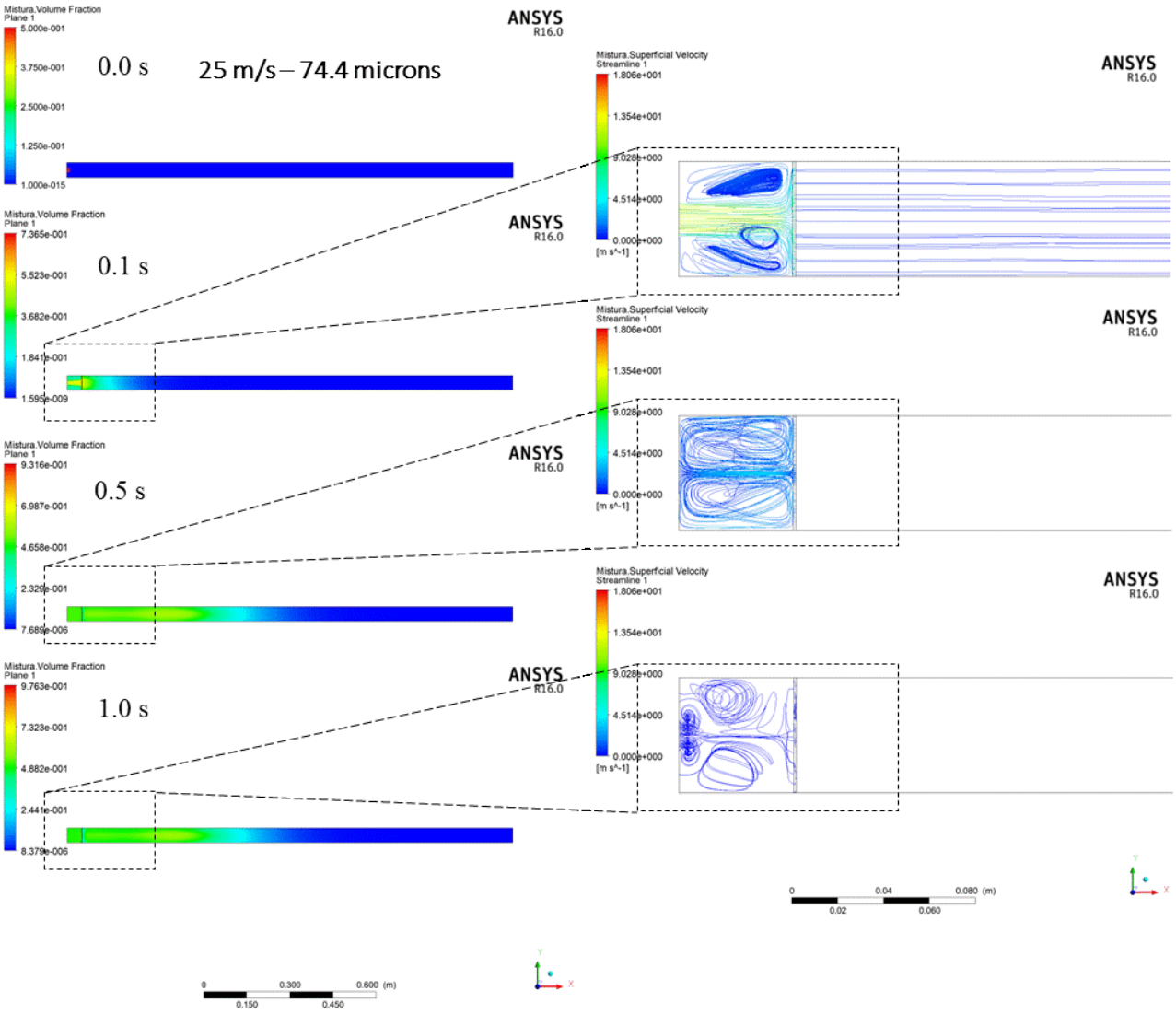

Figure 11: Flow in the windpipe for a velocity of 25 m/s at 74.4 µm particle size.

Comparison of model with real data

The applied model shows that, for all applied particle velocities and sizes, the presence of the physical barrier reduces both the amount of droplets that permeate the wind tunnel and the distance traveled by them. These results are in agreement with empirical observations and experimental results, discussed below.

Amendola and collaborators [32], using equipment that mimics the breathing process, showed that surgical masks are capable of retaining more than 97% of particles larger than 0.28 µm. The speed of propagation of air expelled during breathing, 1.4 m/s [28], approaches the lowest flow value applied in the simulation referring to speech, and this is translated into the close correlation between the experimental result, 97 to 100% [32], and that predicted by the model (above 90%).

Simulation data shows that increasing speed reduces the amount of material retained in the filter material. For the same particle size (74 µm), the volumetric fraction in the filter media is reduced by 25.1% when the velocity increases to 3.2 for 10 m/s, 28.3% for 20 m/s, and 40.7% to 25 m/s. This reduction in filtration efficiency as a function of particle flow is supported by experimental data [33, 11, 34], which confirm the high impact that velocity has on the particle holding capacity of the filter media.

As previously presented, when the speech velocity (3.4 m/s) is applied, the small number of particles that pass through the filter medium reach a maximum distance of 5 cm downstream of the filter medium. Radney and collaborators [35], using an apparatus formed by a filtering membrane and a PVC pipe on a wooden support, demonstrated that, at low speeds, the behavior predicted by the model presented here is the same as that observed in the laboratory, with no particles at distances greater than 5 cm when the filter medium is applied.

About the protective effect of the mask when particles are expelled at higher velocity, the 40 cm limit for most droplets is validated both by experimental data and other simulation results. In the model proposed by Dbouk and Drikakis [36] it is suggested that, when the filtering membrane is used, even though some particles can reach distances of up to 1.2 m, most of the fluid loses speed and reaches a maximum distance of 35 cm. These predicted maximum distances are similar in closed box and benchtop, which demonstrated that, when surgical masks are used, the few particles able to pass through the membrane were concentrated up to 1 foot (~30 cm) downstream of the filter medium [37].

Table 3 shows how the results of the model applied in the present work relate to experimental data available in the literature.

Table 3 - Comparison between the data generated by the model of the present work and results of real experiments.

Parameters	**Simulation**	**Experimental data**	**Reference**
Adsorptive capacity at low propagation speed	> 90 %	97 – 100 %	[32]
Reduction of the volumetric fraction in the filter medium due to the increase in the injection speed	> 40 %	> 50 %	[33]; [11]; [34]
Maximum distance traveled downstream of the filter medium at low injection speed	5 cm	5 cm	[35]
Maximum distance traveled downstream of the filter media at high injection speed	40 cm	35 cm* 30 cm	[36] [37]

* Mimetic model based on data from real experiments

Conclusions

The Euler-Euler modeling represented the dispersion of expiratory particles in the presence and absence of a filter medium and allowed presenting the efficiency of the porous barrier in controlling the dissemination of particles, which could carry viral pathogens. It was also possible to analyze the influence of the diameter of fluid particles in the medium, where smaller diameters are easily carried by the air, but are subject to saturate the filter medium and undergo recirculation upstream of the filter and slow down, while larger particles can quickly saturate the pores of the material and detach, especially when subjected to high speeds, increasing the rate of contamination of the environment. The flow velocity proved to be another interference factor in the volume of fluid accumulated in the filter material, making it reach saturation faster for higher particle entry rates in the system. Furthermore, it was possible to observe, through comparison of computational data with results of experiments published in the literature, that the proposed modeling fits real situations. Therefore, considering the simulated model, it was possible to infer the positive influence of the use of porous filtration systems, including as PPE, reducing the contamination of fluid particles after the safety distance of one and a half meters to values close to zero, allowing to present the filter material as a potential mitigating agent of viral transmission.

Ethics approval and consent to participate
Not applicable

Data Availability
A data availability statement is compulsory for research articles and clinical trials. Here, authors must describe how readers can access the data underlying the findings of the study, giving links to online repositories and providing deposition codes where applicable.

Conflicts of Interest
The authors declare that there is no conflict of interest regarding the publication of this paper.

Funding Statement
Federal University of Alagoas [1]

Conselho Nacional de Desenvolvimento Científico e Tecnológico (CNPq) [1]

Authors' contributions
APM – Elaborated the design and construction of numerical mesh and carried out the mathematical modeling of the problem.
AASN - Proceed with numerical simulations;
EJSF – Worked on the literature review that composed the introduction;
VBB - Conducted a literary validation survey;
LFAMO - Worked on the literature review that composed the introduction;
JLSD - Translated the text and acted in the revision;
LMTMO - Managed the tasks, wrote the methodology and discussed the results;

Acknowledgments
The authors thank the Federal University of Alagoas and the National Concil for Scientific and Technological Development (CNPq) for the physical structure and financial support.

References

1. KIM, D.; LEE, C.; CHOI, C.; AHN, S.; KIM, I. S**. Transport analysis of particulate matter in media-saturated mesh tube filter for the desalination primary pretreatment process**. Desalination, 495 (1), 114642, 2020.
2. DU, J.; LIU, C.; YIN, S.; REHMAN, A.; DING, Y.; WANG, L. **Particle Size distribution in a granular bed filter**. Particuology, 58, p. 108-117, 2021.
3. WU, S.; CAI, R.; ZHANG, L. **Research progress on the cleaning and regeneration of PM2.5 filter media**. Particuology, 57, p. 28-44, 2021.
4. INTERNATIONAL COMMISSION ON THE FUTURES OF EDUCATION. **Protecting and Transforming Education for Shared Futures and Common Humanity**, 2020.
5. WERNECK, G. L.; CARVALHO, M. S.; **A pandemia de COVID-19 no Brasil: crônica de uma crise sanitária anunciada.** Reports in Public Health, 36 (5), 2020.
6. CENTERS FOR DISEASE CONTROL (CDC). **CDC Guidelines on Social Distancing**, 2020.
7. QURESHI, N. JONES, R. TEMPLE, J. P. J. LARWOOD, T. GREENHALGH, AND L. BOUROUIBA, **What is the evidence to support the 2-metre social distancing rule to reduce COVID-19 transmission?,** 2020.
8. FILLINGHAM, Y. A; GROSSO, M. J.; YATES, A. J.; AUSTIN, M. S. Personal Protective Equipment: Current Best Practices for Orthopaedic Teams. The Journal of Arthroplasty, 35 (7), p. 19 -22, 2020.
9. MONTOYA, M. P.; CHITILIAN, H. V. **Extubation barrier drape to minimize droplet spread**. British Journal of Anaesthesia, 125 (1), p. 195 – 196, 2020.3
10. Howard J, Huang A, Li Z, Tufekci Z, Zdimal V, van der Westhuizen HM, von Delft A, Price A, Fridman L, Tang LH, Tang V, Watson GL, Bax CE, Shaikh R, Questier F, Hernandez D, Chu LF,

Ramirez CM, Rimoin AW. **An evidence review of face masks against COVID-19**. Proceedings of the National Academy of Sciences USA, 118 (4), p. 1-8, 2020.
11. KONDA, A.; PRAKASH, A.; MOSS, G. A. SCHMOLDT, M.; GRANT, G. D.; GUHA, S. **Aerosol filtration efficiency of common fabrics used in respiratory cloth masks**. ACS Nano, 14, p. 6339−6347, 2020. https://dx.doi.org/10.1021/acsnano.0c03252
12. TCHARKHTCHI, A.; ABBASNEZHAD, N.; SEYDANI, M. Z.; ZIRAK, N.; FARZANEH, S.; SHIRINBAYAN, M**. An Overview of filtration efficiency through the masks: Mechanisms of the aerosols penetration**. Bioactive Materials, 6, p. 106 – 122, 2021.
13. Han ZY, Weng WG, Huang QY. **Characterizations of particle size distribution of the droplets exhaled by sneeze.** Journal of The Royal Society Interface, 10 (88), 2013.
14. TANG, Y.; GUO, B. **Computational fluid dynamics simulation of aerosol transport and deposition**. Frontiers of Environmental Science and Engineering, 5(3), p. 363-377, 2011.
15. Leonard, S.; Strasser, W. Whittle, J. et al. **Reducing aerosol dispersion by high flow therapy in COVID-19: High resolution computational fluid dynamics simulations of particle behavior during high velocity nasal insufflation with simple surgical mask**. Jacep Open, 1 (4), p. 1-14, 2020.
16. QIAN, F.; HUANG, N.; ZHU, X.; LU, J. **Numerical Study of the gas-solid flow characteristics of fibrous media based on SEM using CFD-DEM**. Powder Technology, 249, p. 63-70, 2013.
17. MARIAN; MAGAR, A.; JOSHI, M.; RAJAGOPAL, P. S.; KHAN, A.; RAO, M. M.; SAPRA, B. K. **CFD Simulation of the Airborne Transmission of COVID-19 Vectors Emitted During Respiratory Mechanisms: Revisiting the Concept of Safe Distance**. ACS Omega, 6(26), p. 16876-16889, 2021.
18. ZHOU, L.; AYEH, S. K.; CHIDAMBARAM, V.; KARAKOUSIS, P. C. **Modes of Transmission of SARS-COV-2 and evidence for preventive behavioral interventions**. BMC Infectious Diseases, 21, 2021.
19. AUSTRALIAN GOVERNMENT DEPARTMENT OF HEALTH, **Physical distancing for coronavirus (COVID-19),** 2020.
20. GOMES, A. O. C.; TEIXEIRA, A. C. M. S.; TRINDADE, S. H. K.; TRINDADE, I. E. K. **Nasal Cavity Geometry of Healthy Adults Assessed Using Acoustic Rhinometry.** Revista Brasileira de Otorrinolaringologia, 74(5), p. 746-754, 2008.
21. ANSYS CFX - Solver Theory Guide (2010) ANSYS INC. UK.
22. HAMDAOUI, MOHAMED; ACHOUR, NESMA; BEN NASRALLAH, SASSI. **The Influence of Woven Fabric Structure on Kinetics of Water Sorption.** Journal of Engineered Fibers and Fabrics, 9(1), p. 101-106, 2014.
23. PORTARAPILLO, M.; BENEDETTO, A. D. **Methodology for risk assessment of COVID-19 pandemic propagation**. Journal of Loss Prevention in the Process Industries, 72, p. 104584, 2021.
24. JANOSZEK, T.; LUBOSIK, Z.; SWIERCZEK, L.; WALENTEK, A.; JAROSZEWICZ, J. **Experimental and CFD Simulation of the Aerosol Flow in the Air Ventilating the Underground Excavation in Terms of SARS-COV-2 Transmission**. Energies, 14, p. 1-23, 2021.
25. PAWAR, S. B. **CFD Analysis of flow regimes in airlift reactor using Eulerian-Lagrangian approach**. The Canadian Journal of Chemical Engineering, 95(3), p. 420-431, 2016.
26. JAKŠIĆ, DANILO; JAKŠIĆ, NIKOLA. **The porosity of masks used in medicine.** Tekstilec, 47, p. 301-304, 2004.
27. KOTB, H., KHALIL, E.E..**Sneeze and cough pathogens migration inside aircraft cabins**, Rehva, 2, p. 36-45, 2020.
28. TANG, J. W.; NICOLLE, A. D.; KLETTNER, C. A.; PANTELIC, J.; WANG, L.; SUHAIMI, A. B.; TAN, A. Y. L.; ONG, G. W. X.; SU, R.; SEKHAR, C.; CHEONG, D. D. W.; THAM, K. W. **Airflow dynamics of human jets: sneezing and breathing – Potential of infectious aerosols.** Plos One. 8, 4, 59970, 2013. https://doi.org/10.1371/journal.pone.0059970
29. Kwon SB, Park J, Jang J, Cho Y, Park DS, Kim C, Bae GN, Jang A. **Study on the initial velocity distribution of exhaled air from coughing and speaking**. Chemosphere. 2012 Jun;87(11):1260-4. doi: 10.1016/j.chemosphere.2012.01.032.

30. FONTES, D.; REYES, J.; AHMED, K.; KINZEL, M. A study of fluid dynamics and human physiology factors driving droplet dispersion from a human sneeze. Physics of Fluids, 32, 111904, 2020.
31. Sankhyan S, Heinselman K N, Ciesielski P N, Barnes T, Himmel M E, Teed H, Patel S, Vance M E (2021). Filtration Performance of Layering Masks and Face Coverings and the Reusability of Cotton Masks after Repeated Washing and Drying. Aerosol Air Qual. Res. 21: 210117. https://doi.org/10.4209/aaqr.210117.
32. AMENDOLA, L.; SAURINI, M. T.; GIROLAMO, F. D.; ARDUINI, F. **A rapid screening method for testing the efficiency of masks in breaking down aerosols**. Microchemical Journal, 157, p. 104928, 2020. https://doi.org/10.1016/j.microc.2020.104928
33. RENGASAMY, S; EIMER, B.; SHAFFER, R. E. **Simple respiratory protection-- evaluation of the filtration performance of cloth masks and common fabric materials against 20-1000 nm size particles.** The Annals of Occupational Hygiene, 54, 7, p. 789–798, 2010, https://doi.org/10.1093/annhyg/meq044
34. O'KELLY, E.; PIROG, S.; WARD, J.; CLARKSON, P. J. **Ability of fabric face mask materials to filter ultrafine particles at coughing velocity.** BMJ Open, 10, 2020. https://doi:10.1136/bmjopen-2020-039424
35. RADNEY, J. G.; WEAVER, J. L.; VICENZI, E. P.; STAYMATES, M. E.; ZANGMEISTER, C.D. **Filter Inserts Impact Cloth Mask Performance against Nano- to Micro-Sized Particles**. ACS Nano, 15, p. 12860−12868, 2021. https://doi.org/10.1021/acsnano.1c05182
36. Dbouk T., Drikakis D. On pollen and airborne virus transmission. Physics and Fluids, 33, 063313, 2021. https://doi.org/10.1063/5.0055845
37. KOLEWE, E. L.; STILLMAN, Z.; WOODWARD, I. R.; FROMEN, C. A. **Check the gap: Facemask performance and exhaled aerosol distributions around the wearer.** PLoS ONE, 15, 12, 2020. https://doi.org/10.1371/journal.pone.0243885